Inorg. Chem. **2005**, *44*, 9652–9659

MXAN Analysis of the XANES Energy Region of a Mononuclear Copper Complex: Applications to Bioinorganic Systems

Ritimukta Sarangi,[†] Maurizio Benfatto,*[,‡] Kuniko Hayakawa,[‡] Luigi Bubacco,[⊥] Edward I. Solomon,[†] Keith O. Hodgson,[†,§] and Britt Hedman*[,§]

Department of Chemistry, Stanford University, Stanford, California 94305, Laboratori Nazionali di Frascati dell' INFN, C.P. 13, I-00044 Frascati, Italy, Dipartimento di Biologia, Via U. Bassi, Università di Padova, I-30121 Padova, Italy, and Stanford Synchrotron Radiation Laboratory, SLAC, Stanford University, Stanford, California 94309

Received May 4, 2005

The near edge XAS spectra of the mononuclear copper complex $[Cu(TMPA)(OH_2)](ClO_4)_2$ (**1**) have been simulated using the multiple scattering edge simulation package MXAN (or Minuit XANes). These simulations, which employ the muffin-tin (MT) approximation, have been compared to simulations generated using the finite-difference method (FDM) to evaluate the effect of MT corrections. The sensitivity of the MXAN method was tested using structural models that included several different variations on the bond angles and bond distances for the first-shell atoms of **1**. The sensitivity to small structural changes was also evaluated by comparing MXAN simulations of **1** and of structurally modified $[Cu(TMPA)(L)]^{n+}$ complexes [where L = –O–$(F_8TPP)Fe^{III}$, –F, –OPO_2(O-*p*-nitrophenyl)Zn^{II}-(TMPA), and –NCMe] to the experimental data. The accuracy of the bond distances obtained from the MXAN simulations was then examined by comparison to the metrics of the crystal structures. The results show that MXAN can successfully extract geometric information from the edge structure of an XAS spectrum. The systematic application of MXAN to **1** indicates that this approach is sensitive to small structural changes in the molecule that are manifested in the XAS edge spectrum. These results represent the first step toward the application of this methodology to bioinorganic and biological systems.

Introduction

X-ray absorption spectroscopy, in particular extended X-ray absorption fine structure (EXAFS), is a powerful experimental technique for local structure determination,[1−4] which has been successfully applied to problems in a broad range of scientific fields, such as biology, chemistry, material science, and surface science.[2,5−7] Continuing developments in synchrotron radiation sources, beam line optics, detectors, and data analysis methods have improved the resolution and accuracy of the EXAFS technique. Although EXAFS can be applied to a variety of systems in solution, crystalline, or amorphous forms, there are several limitations with particular relevance to biological systems. (A) Many metalloenzymes cannot be isolated at high enough concentrations to obtain EXAFS data to a reasonable *k*-range, or in some cases, beam damage/photoreduction prevent data of sufficient signal-to-noise to be obtained. (B) Protein active sites undergo chemical, electronic, and/or structural changes during their mechanistic pathway that involve the formation of reactive intermediates. Structural details of these intermediates can provide important information regarding the overall function of the protein. These intermediates, however, can be difficult to trap and are usually extremely short-lived. The time

* To whom correspondence should be addressed. E-mail: hedman@ssrl.slac.stanford.edu (B.H.); Maurizio.Benfatto@lnf.infn.it (M.B).
[†] Department of Chemistry, Stanford University.
[‡] Laboratori Nazionali di Frascati dell' INFN.
[⊥] Università di Padova.
[§] Stanford Synchrotron Radiation Laboratory, SLAC, Stanford University.

(1) Zhang, H. H.; Hedman, B.; Hodgson, K. O. In *Inorganic Electronic Structure and Spectroscopy, Volume 1: Methodology*; Solomon, E. I., Lever, A. B. P., Eds.; John Wiley and Sons: New York, 1999; pp 514−554.
(2) Cramer, S. P.; Hodgson, K. O. *Prog. Inorg. Chem.* **1979**, *25*, 1−79.
(3) Fonda, L. *J. Phys.: Condens. Matter* **1992**, *4*, 8269−8302.
(4) Teo, B. K. *EXAFS: Basic Principles and Data Analysis*; Springer-Verlag: New York, 1986.
(5) Iwasawa, Y. *X-ray Absorption Fine Structure for Catalysis and Surfaces*; World Scientific: River Edge, NJ, 1996; Vol. 2.
(6) Stern, E. A. In *EXAFS, SEXAFS and XANES*; Koningsberger, D. C., Prins, R., Eds.; John Wiley and Sons: New York, 1988; Vol. 1.
(7) Crozier, E. D. *Nucl. Instrum. Methods, B* **1997**, *133*, 134−144.

10.1021/ic050703n CCC: $30.25
Published on Web 11/23/2005

required for EXAFS data collection can limit the successful application to these short-lived intermediates.

XANES (X-ray absorption near edge structure) is extremely sensitive to the geometric environment of the absorbing atom.[8,9] A quantitative analysis of the XANES, which includes the rising edge and ~200 eV above it, can address some of the aforementioned shortcomings of EXAFS. A structural analysis that exploits XANES data can avoid the low signal-to-noise ratio problem encountered at high *k*, and XANES spectra can be accumulated quickly. In this study, we apply MXAN (Minuit XANes), a XANES fitting routine, to the Cu K-edge XAS of $[Cu^{II}(TMPA)(OH_2)](ClO_4)_2$ (**1**).[10] The $[Cu^{II}(TMPA)]$ moiety has been coupled to an Fe−porphyrinate system to synthesize a coupled mixed binuclear heme−copper complex,[11] which models the structural aspects of the binuclear active site in the heme−copper oxidase super-family, which includes cytochrome *c* and quinol oxidases.[12−15] Cytochrome *c* oxidase (C*c*O) catalyzes the terminal step in respiration; the $4e^-/4H^+$ reduction of dioxygen to H_2O.[16,17] This process is coupled with transmembrane proton translocation, in which these membrane-spanning proteins provide the driving force for ATP synthesis.[18,19]

The $[Cu^{II}(TMPA)]$ moiety mimics the Cu_B site present in the active site for O_2 reduction in C*c*O.[20] The molecule is trigonal bipyramidal with the equatorial positions occupied by pyridine nitrogens and the axial positions by aliphatic nitrogen and water (Figure 1). The complex was chosen mainly for two reasons: (1) The TMPA ligand system provides strong multiple scattering which furnishes a rich edge structure to simulate. (2) A number of monomeric, homo-dimeric, and hetero-dimeric $[Cu^{II}(TMPA)L]^{n+}$ complexes have been synthesized and have crystal structures available. Although MXAN has successfully been applied to unknown structures,[21,22] the known structures utilized here allow for the evaluation of the impact of ligand variations on fit results using single-point MXAN calculations. This study provides a critical test of the MXAN method through comparison of the simulation results to crystallographic data. The successful treatment of this complex model system using MXAN allows extension of this method to other bioinorganic and biological systems.

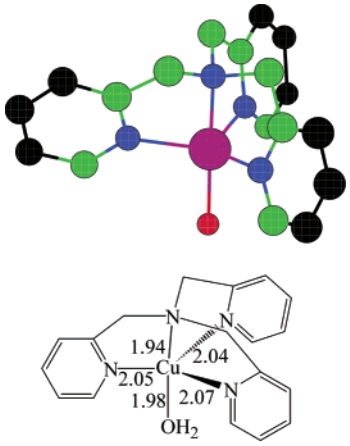

Figure 1. Crystal structure of $[Cu^{II}(TMPA)OH_2](ClO_4)_2$ with distances (Å). Carbons represented in green were used in the 15-atom fit, while the carbon atoms added to comprise the 23-atom cluster are shown in black (Figure 2 and see text).

Experimental Section

The X-ray absorption spectra of **1** were measured at the Stanford Synchrotron Radiation Laboratory on the focused 16-pole 2.0 T wiggler beam line 9−3 under standard ring conditions of 3 GeV and 60−100 mA. A Si(220) double-crystal monochromator was used for energy selection. ***Warning!*** *Perchlorates are classified as class A explosives, and organopercholorates are potentially explosive if strongly heated or shocked. Proper care was taken during handling of* $[Cu^{II}TMPA(OH_2)(ClO_4)$ *during XAS sample preparation.* The solid sample preparation, mode of data collection, and achievement of internal calibration have been described in earlier publications.[1] Data presented here represent a two-scan average spectrum, which was processed by fitting a second-order polynomial to the pre-edge region and subtracting this from the entire spectrum as background. A three-region spline of orders 2, 3, and 3 was used to model the smoothly decaying post-edge region. The data were normalized by subtracting the spline and by assigning the edge jump to 1.0 at 9000 eV using the SPLINE program in the XFIT suite of programs.[23]

For MXAN analysis, the fits were typically performed over the energy range from −10 to 150 or 200 eV (0 eV is defined at 9000 eV). This range includes the EXAFS region to $k = \sim 7$ Å^{-1}. In the refinements, all atoms belonging to each pyridine ring were moved rigidly linked to the N atom coordinated to copper. Additionally, the three carbon atoms of the tertiary amine of the TMPA moiety were rigidly linked to its Cu-coordinated N during the fitting. Thus, the number of free structural parameters was restricted to 5−15 depending on if angular motion was included. The MXAN simulations were performed by alternative fitting of all the structural

(8) Benfatto, M.; Della Longa, S. *J. Synchrotron Rad.* **2001**, *8*, 1087−1094.
(9) Kau, L.-S.; Spira-Solomon, D. J.; Penner-Hahn, J. E.; Hodgson, K. O.; Solomon, E. I. *J. Am. Chem. Soc.* **1987**, *109*, 6433−6442.
(10) Nagao, H.; Komeda, N.; Mukaida, M.; Suzuki, M.; Tanaka, K. *Inorg. Chem.* **1996**, *35*, 6809−6815.
(11) Ghiladi, R. A.; Hatwell, K. R.; Karlin, K. D.; Huang, H.; Moënne-Loccoz, P.; Krebs, C.; Huynh, B. H.; Marzilli, L. A.; Cotter, R. J.; Kaderli, S.; Zuberbühler, A. D. *J. Am. Chem. Soc.* **2001**, *123*, 6183−6184.
(12) Yoshikawa, S.; Shinzawa-Itoh, K.; Nakashima, R.; Yaono, R.; Yamashita, E.; Inoue, N.; Yao, M.; Fei, M. J.; Libeu, C. P.; Mizushima, T.; Yamaguchi, H.; Tomizaki, T.; Tsukihara, T. *Science* **1998**, *280*, 1723−1729.
(13) Tsukihara, T.; Aoyama, H.; Yamashita, E.; Tomizaki, T.; Yamaguchi, H.; Shinzawa-Itoh, K.; Nakashima, R.; Yaono, R.; Yoshikawa, S. *Science* **1995**, *269*, 1069−1074.
(14) Tsukihara, T.; Aoyama, H.; Yamashita, E.; Tomizaki, T.; Yamaguchi, H.; Shinzawa-Itoh, K.; Nakashima, R.; Yaono, R.; Yoshikawa, S. *Science* **1996**, *272*, 1136−1144.
(15) Iwata, S.; Ostermeier, C.; Ludwig, B.; Michel, H. *Nature* **1995**, *376*, 660−669.
(16) Calhoun, M. W.; Thomas, J. W.; Gennis, R. B. *Trends Biochem. Sci.* **1994**, *19*, 325−331.
(17) García-Horsman, J. A.; Barquera, B.; Rumbley, J.; Ma, J. X.; Gennis, R. B. *J. Bacteriol.* **1994**, *176*, 5587−5600.
(18) Malmström, B. G. *Chem. Rev.* **1990**, *90*, 1247−1260.
(19) Ferguson-Miller, S.; Babcock, G. T. *Chem. Rev.* **1996**, *96*, 2889−2907.
(20) Kim, E.; Chufàn, E. E.; Kamaraj, K.; Karlin, K. D. *Chem. Rev.* **2004**, *104*, 1077−1133.
(21) Sepulcre, F.; Proietti, M. G.; Benfatto, M.; Della Longa, S.; García, J.; Padrós, E. *Biophys. J.* **2004**, *87*, 513−520.
(22) Frank, P.; Benfatto, M.; Szilagyi, R. K.; D'Angelo, P.; Della Longa, S.; Hodgson, K. O. *Inorg. Chem.* **2005**, *44*, 1922−1933.
(23) Ellis, P. J.; Freeman, H. C. *J. Synchrotron Rad.* **1995**, *2*, 190−195.

and all the nonstructural parameters (vide infra) until the global minimum was reached.

In standard EXAFS analysis, the evaluation of the number of independent parameters is done through the so-called Stern's criterion ($n < 2 + 2\delta k \delta R/\pi$).[24] This criterion cannot be applied in the edge region, as in this case, the exact inversion of the scattering path operator has to be used. The fitting is performed over an energy range (the edge-region) where either a series expansion (used for EXAFS) cannot be applied, or several multiple scattering signals of very high order give sizable contributions (the region above the edge). The number of independent parameters can, however, be estimated case-by-case through evaluation of both the covariance matrix and the contour plots related to the structural parameters of the subspace chosen for the fitting via the subroutines in the MINUIT program[25,26] using the MIGRAD and HESSE subroutines. In the fits, the values of the correlation between the structural parameters were consistently very small and their effects are reflected in the reported errors.

For EXAFS analysis, full-range theoretical signals, $\chi(k)$, were calculated using FEFF (version 7.0)[27,28] and fit to the data using EXAFSPAK.[29] The structural parameters varied during the fitting process were the bond distance (R) and the bond variance (σ^2), which is related to the Debye−Waller factor resulting from thermal motion, and static disorder. The nonstructural parameter E_0 (the energy at which $k = 0$) was also allowed to vary but was restricted to a common value for every component in a given fit. Coordination numbers were systematically varied in the course of the fit but were fixed within a given fit.

Theoretical Details. MXAN is a new software procedure[8] capable of performing a quantitative analysis of the XANES energy region with the aim of deriving structural information. The method is based on the comparison between experimental data and theoretical calculations, performed by varying selected structural parameters starting from a well-defined initial geometrical configuration around the absorber. The iterative calculation of XANES spectra with several geometrical configurations, to obtain the best fit to the experimental data, is achieved in a reasonable amount of time and the optimization parameter space is achieved by the minimization of the square residual function, also in parameter space.

The calculations are performed within the so-called full MS (multiple scattering) approach, i.e., the inverse of the scattering path operator is computed exactly, avoiding any 'a-priori' selection of the relevant MS paths. The MXAN procedure uses the set of programs developed by the Frascati theory group; in particular VGEN, a generator of muffin-tin (MT) potentials, and the CONTINUUM code for the full MS cross-section calculation. The optimization in parameter space is achieved using the MINUIT routines of the CERN library by minimizing the square residual function (eq 1).

$$R_{sq} = n \frac{\sum_{i=1}^{m} w_i[(y_i^{th} - y_i^{exp})\epsilon_i^{-1}]^2}{\sum_{i=1}^{m} w_i} \qquad (1)$$

In eq 1, n is the number of independent parameters, m is the number of data points, y_i^{th} and y_i^{exp} are the theoretical and experimental values of absorption, respectively, ϵ_i is the individual error in the experimental data set, and w_i is a statistical weight. For w_i = constant = 1, the square residual function, R_{sq}, becomes the statistical χ^2 function. In this paper, we assume a constant experimental error, $\epsilon = 0.9\%$, for the whole experimental data set.

The MXAN method is based on the MT approximation for the shape of the potential and uses a complex optical potential, based on the local density approximation of the self-energy of the excited photoelectron.[30] The MT radii are chosen according to the Norman criterion, with specified percentage of overlap, and the potential is recalculated at each step of the minimization procedure, keeping the overlap factor fixed. The effects of the non-MT corrections will be discussed in some details later in this paper, but their effect is confined within the first 20−30 eV of the edge[31,32] and thus has very limited influence on the structural determination[33] due to the relatively large energy range used in the fit. In this way, the geometrical arrangements restrain the numerical results of the fitting procedure.

The self-energy is calculated in the framework of the Hedin−Lundqvist (HL) scheme. To avoid the relevant overdamping at low energies in the case of covalent molecular systems, MXAN uses a phenomenological approach to calculate the inelastic losses on the basis of a convolution of the theoretical spectrum. This calculation uses only the real part of the HL potential, with a suitable Lorentzian function having an energy-dependent width of the form $\Gamma_{tot}(E) = \Gamma_c + \Gamma_{mfp}(E)$. The constant part, Γ_c, includes the core hole lifetime and the experimental resolution, while the energy-dependent term, $\Gamma_{mfp}(E)$, represents all the intrinsic and extrinsic inelastic processes. The $\Gamma_{mfp}(E)$ function is zero below an onset energy, E_s (which in extended systems corresponds to the plasmon excitation energy), and begins to increase from a value, A_s, following the universal functional form of the mean free path in solids. Both the onset energy E_s and the jump A_s are introduced in the $\Gamma_{tot}(E)$ function via an arctangent functional to avoid discontinuities and to simulate the electron−hole pair excitations.[34] Their numerical values are derived at each computational step (i.e., for each geometric configuration) on the basis of a Monte Carlo fit, similar to the procedure used in optimization by simulated annealing. Application of this procedure to different systems confirm the reliability of our phenomenological approach to the treatment of inelastic losses in the XANES spectrum.[35]

This phenomenological approach can be justified on the basis of a multichannel multiple scattering theory.[36] In the limit of the sudden approximation, the net absorption is given by a sum over all the possible excited states of the ($N - 1$) electron system. By assuming that the channels arising from the excitation of the ($N - 1$) electrons are near in energy, the total absorption is given by a

(24) Stern, E. A. *Phys.: Rev. B.* **1993**, *48*, 9825−9827.
(25) Filipponi, A. *J. Phys.: Condens. Matter* **1995**, *7*, 9343−9356.
(26) Michalowicz, A.; Vlaic, G. *J. Synchrotron Rad.* **1998**, *5*, 1317−1320.
(27) Muestre de Leon, J.; Rehr, J. J.; Zabinsky, S. I.; Albers, R. C. *Phys. Rev. B.* **1991**, *44*, 4146−4156.
(28) Rehr, J. J.; Muestre de Leon, J.; Zabinsky, S. I.; Albers, R. C. *J. Am. Chem. Soc.* **1991**, *113*, 5135−5140.
(29) George, G. N. *EXAFSPAK* and *EDG_FIT*; Stanford Synchrotron Radiation Laboratory, Stanford Linear Accelerator Center, Stanford University, Stanford, CA 94309, 2000.
(30) Tyson, T. A.; Hodgson, K. O.; Natoli, C. R.; Benfatto, M. *Phys. Rev. B* **1992**, *46*, 5997−6019.
(31) Joly, Y. *Phys. Rev. B* **2001**, *63*, 125120−125110.
(32) Cabaret, D.; Joly, Y.; Renevier, H.; Natoli, C. R. *J. Synchrotron Rad.* **1999**, *6*, 258−260.
(33) Hayakawa, K.; Hatada, K.; D'Angelo, P.; Della Longa, S.; Natoli, C. R.; Benfatto, M. *J. Am. Chem. Soc.* **2004**, *126*, 15618−15623.
(34) Della Longa, S.; Arcovito, A.; Girasole, M.; Hazemann, J. L.; Benfatto, M. *Phys. Rev. Lett.* **2001**, *87*, 155501−155504.
(35) D'Angelo, P.; Benfatto, M.; Della Longa, S.; Pavel, N. V. *Phys. Rev. B* **2002**, *66*, 064209−064207.
(36) Benfatto, M.; Della Longa, S.; D'Angelo, P. *Phys. Scr.* **2005**, *T115*, 28−30.

convolution of the one-particle spectrum, calculated with the full-relaxed potential, with a spectral function, $A(\omega)$, representing the weight of the other excited states. Hence, the total XAS cross-section can be written as

$$\mu = \sum_n \mu_n \xrightarrow{\Delta E \to 0} \int \mu(\omega - \omega')A(\omega')\,d\omega' \qquad (2)$$

where the Lorentzian function previously defined is assumed to approximate the spectral function $A(\omega)$. This is exactly equivalent, within the approximations of locality and homogeneous system, to the use of a Green's function approach with a G_0 obeying Dyson's equation with a suitable local complex optical potential. Therefore, the $\Gamma_{tot}(E)$ function is characterized by parameters that have clear physical meanings and are varied within a well-defined interval. Obviously, when contributions from one or more of these excited states become relevant, they must be considered explicitly in the calculations.

The MXAN method introduces four nonstructural parameters,[34,36] three of which are related to the damping procedure, although Γ_c can be derived from the core-hole lifetime and the experimental resolution. The fourth is the overlap factor of the MT radii. Many applications to different test cases indicate that the correlation between structural and nonstructural parameters is small, with a very limited effect on the structural reconstruction essentially limited to the evaluation of the statistical error of the structural parameters.[35]

Recently, the MXAN program was modified to read an external theoretical spectrum, for example, the one obtained with the finite difference method (FDM), and to perform a minimization only in the nonstructural parameter space. In this way, a suitable quantitative comparison between different theoretical methods can be easily made.

The FDM provides an approach to solve the Schrödinger equation (SE) with a potential of general shape (without the MT approximation) when working in the framework of the local density approximation. Although the first formulation[37] was given in the 1930s, this method has only recently found practical application due to the large amount of computational time needed for the numerical calculation. This method solves differential equations by making them discreet over a grid of points that fill the volume on which calculation is made. In the study of the molecular complex presented here, the SE of a spherical volume centered on the absorbing atom[31] is needed.

The quantity to be calculated is the value of the wave function $\psi_i = \psi(r_i)$ on each grid point, i, given a local potential $V_i = V(r_i)$ defined in the same grid as the sum of the Coulomb and the exchange−correlation terms. This is given by the real part of the HL potential. Using a suitable numerical expression for the Laplacian, the SE at point i becomes

$$(-I_{ii} + V_i - E)\psi_i + \sum_j^{\text{neighbors}} - I_{ij}\psi_j = 0 \qquad (3)$$

Here, atomic units and Rydbergs are used and I_{ij} indicates a numerical expression for the Laplacian. Both I_{ij} and the sum over the neighbors depend on the degree of the polynomial used to numerically approximate the Laplacian. In the present study, the fourth order has been used. The large system of linear equations connecting the values of the wave function at all points must be solved to obtain the wave function in the whole space and the spectroscopic quantities to be compared with the experimental data.

(37) Kimball, G. E.; Shortley, G. H. *Phys. Rev.* **1934**, *45*, 815−820.

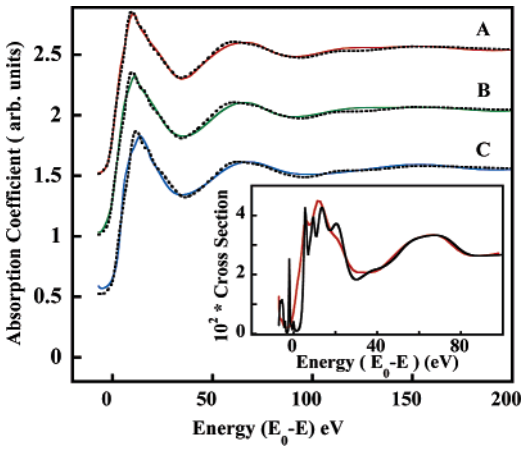

Figure 2. Comparison between experimental data (· · ·) and best-fit MXAN simulations. (A) Simulation using the 23-atom cluster (red). (B) Simulation using the 15-atom cluster (green). (C) FDM simulation using the 15-atom cluster (blue). Inset: FDM (black) and MXAN (red) simulations obtained without convolution factors.

Thus, the smaller the interpoint distance, the more accurate the calculation. In this study, a value of 0.25 Å has been used, providing a reasonable compromise between the computational time and the accuracy of the calculation.[31] To account for inelastic losses, the raw theoretical spectrum was used as input for the MXAN code to exploit the phenomenological method of the MXAN procedure.

Results and Discussions

The basic unit of the bioinorganic complex $[Cu^{II}(TMPA)(OH_2)](ClO_4)_2$ is formed by 23 atoms around the copper (excluding the hydrogens, counterions and water molecules present in the crystal) (Figure 1). This cluster was used as the starting model (using coordinates from the known crystal structure to create the initial parameters) for the MXAN analysis. Figure 2 shows the comparison between the experimental data and a set of calculations performed using the MXAN and the FMD methods. In the first simulation (Figure 2A), the experimental data are compared with the MXAN calculation obtained from refining the nonstructural parameters, in particular the overlap factor between the MT radii. The agreement between the theoretical and experimental data is good in the energy region chosen for the simulations, resulting in $R_{sq} = 3.64$. The overlap factor is ∼5%, the constant part $\Gamma_c = 3.0$ eV, the onset energy $E_s =$ 8.85 eV, and the jump $A_s = 4.95$. The value of Γ_c is reasonable considering that the core-hole lifetime broadening is 1.55 eV, which is further convoluted with the monochromator (experimental) resolution of ∼2.0 eV[38] at 9000 eV. The same analysis was repeated using a smaller cluster formed by 15 atoms, which include atoms within a distance of 3.2 Å from the absorbing Cu center (Figure 1). The result is presented in the second simulation (Figure 2B) showing the comparison between experimental data and theoretical calculation at the best-fit condition. The agreement to the experimental data is still good, indicating that the first-shell neighbors have a dominant contribution to the XANES

(38) Lytle, F. W. In *Applications of Synchrotron Radiation*; Winick, H., Xian, D., Ye, M., Huang, T., Eds.; Gordon and Breach Science Publishers: Langhorne, PA, 1988; Vol. 4, pp 135−223.

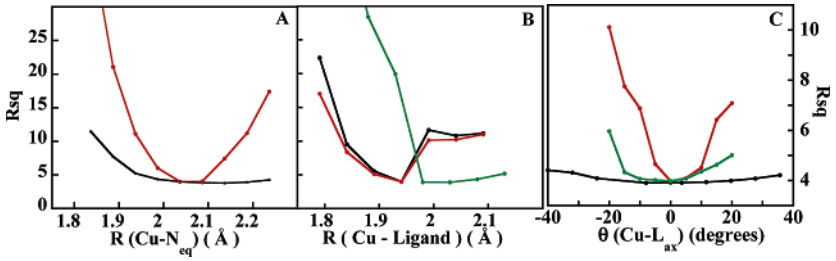

Figure 3. Profiles of R_{sq} dependence on structural parameters. (A) Varying the Cu−N_{eq} distance (R_0 = 2.04 Å) (all other TMPA moieties are fixed) (black) or the Cu−N_{eq} distance (R_0 = 2.04 Å) (all other TMPA moieties move rigidly) (red). (B) Varying the Cu−O distance (green), the Cu−N_{ax} distance (red), and Cu−N_{ax} distance (with three bound carbons moved rigidly) (black). (C) Angle dependence of Cu−L_{ax} oriented along the *z* axis; Cu−O (black), Cu−N_{ax} (green), Cu−N_{ax} (three bonded carbons moved rigidly) (red).

region and that the edge structure could be a signature of the trigonal bipyramidal geometry of **1**. Some discrepancies with the experimental spectrum appears in the low-energy part of the simulation leading to an increase in the error function (R_{sq} = 5.60), demonstrating the sensitivity of the MXAN method to structural detail. The third simulation (Figure 2C) shows the comparison between the experimental data and the FDM calculation performed on the 15-atom cluster. The smaller cluster was chosen to gain reasonable computation time. The output of the FDM calculation, which was performed using the real part of the HL potential, was used as input for the MXAN code to refine the nonstructural damping parameters. The agreement with the experimental data is still rather good, and the error is comparable to the calculation performed including the MT approximation. Figure 2 (inset) shows the comparison between the FDM and MXAN calculations obtained without any convolution to emphasize the effects of non-MT corrections. These effects are dominant in the edge, including 20−30 eV above E_0 of the raw spectrum but become smaller in the convoluted spectrum (see Figure 2B and C). The non-MT corrections have limited influences on the structural fit when the simulation is performed over a relatively large energy range (as used in the MXAN procedure). Over this range, the geometrical parameters dominate the XAS spectrum and restrain the numerical results of the fitting procedure. It is therefore clear that MT approximations are applicable in simulating edge spectra over a relatively large energy region as used in MXAN (∼200 eV above E_0) over which the effects of non-MT corrections are limited. This behavior has a well-defined theoretical basis.

The total photoabsorption cross-section, σ_t, for a local potential of any shape can be written in terms of the MT photoabsorption cross-section, σ_{MT}, as

$$\sigma_t \approx \sigma_{MT} + \mathrm{corr}(E; V_{int}) \quad (4)$$

In other words, the total non-MT cross section can be written as the sum of the cross sections calculated in the MT approximation and a correction term that decreases with the energy and depends on the potential in the interstitial volume. This correction term is small for complexes with low symmetry, as in complex **1**.

The crystal structure of complex **1** also includes several water molecules and two perchlorate counterions in the unit cell. When these molecules are included in the cluster used to generate the simulated spectrum, the R_{sq} value decreases by ∼30%. The contributions from the counterion and H_2O molecules are small but have detectable effects on the fits, although the overall line shape remains the same (data not shown). In this case, Γ_c decreases to 2.77 eV and E_s and A_s are equal to 14.8 and 5.75, respectively.

On the basis of these initial results, a set of systematic simulations were performed to evaluate the contributions of different structural parameters to the edge structure and goodness of fit, R_{sq}. The contributions from the equatorial nitrogen ligands and the axial nitrogen and oxygen were analyzed independently by MXAN. Figure 3 gives the correlations between the analyzed structural parameters and R_{sq}. Figure 3A shows the effect on R_{sq} with individual variations in the Cu−N_{eq} (equatorial nitrogen) distance (the atoms of the pyridine ring were linked to move as a rigid body). This distance profile shows that, for bond distances shorter than the crystallographic distance (R_0), R_{sq} increases significantly, while for distances longer than R_0, the quality of the fit is not significantly affected. On the other hand, when the bond distances for all the three Cu−N_{eq} bonds are linked and varied simultaneously (the pyridine atoms remain linked), the profile of R_{sq} shows a well-defined minimum, in agreement with the crystallographic parameters. Figure 3B shows the effects of systematic variation of the bond distances of the axial ligands. For the Cu−O bond-distance profile, a sharp increase in the R_{sq} is observed for distances shorter than the corresponding R_0, while R_{sq} is insensitive to distances greater than R_0. The Cu−N_{ax} bond distance profile shows a well-defined minimum for R_{sq} at R_0 that increases sharply for distances both shorter and longer than R_0. A sharper minimum is obtained when N_{ax} and the three carbon atoms bound to it are moved as a rigid body. Finally, to explore the angular dependence of the axial ligand position, the molecule was placed in the reference frame with the Cu−N_{ax} and Cu−O bonds along the *z* axis. Variations of the polar angle of the Cu−O bond do not affect the R_{sq} value and seem to have only a limited effect on the simulation (Figure 3C). A more significant effect is observed for the angular dependence of the Cu−N_{ax} bond. This dependence is further enhanced when N_{ax} is linked with the three bonded carbon atoms as a rigid body, and a minimum is obtained at the Cu−N_{ax} R_0 value.

As mentioned in the Experimental Section, structural and nonstructural parameters were varied stepwise, separately

Table 1. First-Shell Bond Distances (Å)

bond	crystal structure	MXAN[a]	EXAFS[b]
Cu−O	1.98	1.97	2.03
Cu−N_{ax}	1.94	1.94	1.91
Cu−N_{eq1}	2.05	2.05	2.03
Cu−N_{eq2}	2.04	2.11	2.03
Cu−N_{eq3}	2.07	2.11	2.03

[a] Distances refined as described in the text following the alternative fitting approach of all the structural and nonstructural parameters. [b] The Cu−O and Cu−N_{eq} distances are not separable by EXAFS (resolution ∼±0.13 Å). The statistical errors in the MXAN procedure evaluated by the MIGRAD routine is ±0.03 Å.

from one another. It is important to mention that these parameters were confirmed to be independent. Figure 3 and related discussion show that if bond lengths were fixed at distances that resulted in a deviation from the best-fit geometry, the nonstructural parameters did not refine to give a better fit or even a comparable fit (as judged by R_{sq}).

The structural model generated was further tested by comparing bond distances to those obtained from the EXAFS analysis. The k^3-weighted EXAFS data and their Fourier transform are shown in Figure S1. Theoretical phase and amplitude parameters for the fit were generated by FEFF, calculated from the crystallographic parameters of **1**. Table S1 summarizes the best-fit parameters. Table 1 summarizes bond distances obtained from the crystal structure, MXAN analysis (including water and counterions), and EXAFS analysis. As observed above, the MXAN analysis is very accurate in determining bond distances of the axial atoms (Figure 3B). A small difference from the crystal structure distances is observed for the equatorial ligands, which is due to the fact that the distances are between 2.04 and 2.07 Å, which, in this case, cannot be resolved by the fitting procedure (Figure 3A). The EXAFS spectrum was measured to $k = 13$ Å^{-1} (∼9644 eV) due to the presence of trace amounts of zinc in the sample (the zinc edge occurs at ∼9659 eV). This is often the case with copper-containing bioinorganic model systems and biological samples, which limits the resolution to ∼0.13 Å ($\Delta r = \pi/(2\Delta k)$). Thus, the first-shell N_{ax} and N_{eq} distances cannot be separated in the EXAFS fit (Table S1).

Although in general MXAN edge analysis will not necessarily provide structural results that are of higher accuracy to those derived from EXAFS analysis, the two methods will show different sensitivity to certain geometric structural parameters (the EXAFS region is uncomplicated by the core potential and is treated as a convolution of sine waves resulting from scattering and backscattering of the ejected photoelectron, whereas the edge region is very much affected by the core potential). Alone, and in particular if combined, MXAN can therefore provide additional information to that of EXAFS analysis in resolving first-shell bond distances, in particular for cases where the EXAFS data are not available to a high k-range.

To further assess contributions from individual structural parameters to the simulated spectral line shape, a set of calculations was performed where individual sections of the starting structure were omitted. Figure 4 shows the comparison of the experimental data and these simulations. In

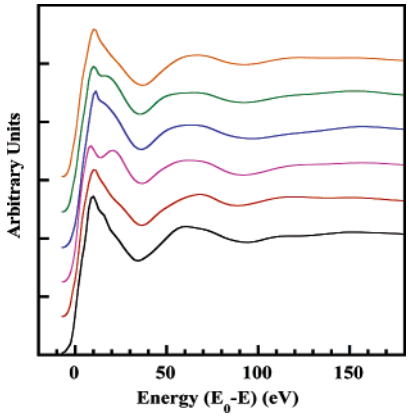

Figure 4. Experimental data (black) and MXAN simulated spectra obtained by removal of the following structural units: axial O (red), axial N (magenta), three carbons bonded to the axial N (but N_{ax} included) (purple), axial N and bonded carbons (green), and one pyridine ring on the equatorial N(orange).

the cluster without the axial oxygen ligand (red line), the most significant effect can be observed at ∼60 eV above the edge. A more-complex effect which spans the whole energy region of the fit is observed when omitting the axial nitrogen (N_{ax}) ligand (purple line). A significant change is observed when the carbons bonded to N_{ax} are omitted from the cluster (blue line). Again, the removal of both N_{ax} and the carbons bonded to N_{ax} result in a line shape (green line) significantly different from the experimental data (black line). This is supported by the strong angular dependence of N_{ax} (vide supra) resulting from a dominant backscattering contribution. Finally, one of the pyridine rings connected to the equatorial nitrogen (N_{eq}) was omitted (orange line); the resulting change in the line shape is small, yet significant enough to be detected by the fitting routine.

A relevant issue in the structural analysis of unknown metalloproteins or in the characterization of reaction intermediates is the identification of the first shell ligands of the metal ion. In a simplified scenario, an attempt was made to evaluate the effect of the ligand type on the line shape of the spectra. Figure 5 shows simulations which involve the systematic change of the axial oxygen to N, S, Cl, and Se at a fixed distance of 1.97 Å (the best-fit Cu−O distance obtained from the MXAN refinement). Replacement of O with N results in very little change in the goodness of simulation in comparison to the data, but replacing O with Cl or S perturbs the simulation significantly in the 20−120 eV energy region. Replacement of O with Se gives a significantly less-accurate simulation, especially in the 100−200 eV energy region. The simulations were then repeated with Cu−L bond distances of 2.0, 2.32, 2.35, and 2.45 Å for N, Cl, S, and Se, respectively. These values were obtained from an average of the bond distances of several relevant structures in the Cambridge Structural Database (CSD).[39] The distances are reasonable on the basis of the change in effective ionic radii of N through Se.[40] Although these single-point simulations better matched the experimental data compared to the simulations performed with a constrained

(39) Allen, F. H. *Acta Crystallogr. B* **2002**, *58*, 380−388.
(40) Shannon, R. D. *Acta Crystallogr. A* **1976**, *32*, 751−767.

Table 2. MXAN Fit Results (R_{sq}) for the Two Model Approaches (Modified and Original) as Described in the Text, Compared to Crystal Structure First-Shell Distances

	bond distances[a] (Å)					error (R_{sq})[d]	
structure	Cu−L	Cu−N(ax)[b]	Cu−N_1(eq)[c]	Cu−N_2(eq)	Cu−N_3(eq)	modified	original
1	1.98	1.94	2.05	2.04	2.07	–	3.64
2a	1.85	2.06	2.04	1.94	2.01	5.1	31.4
2b	1.90	2.15	2.09	1.99	2.06	15.1	12.7
2c	1.99	2.43	2.12	2.07	2.08	21.1	15.9
2d	1.87	2.10	2.17	1.98	2.01	13.5	18.7

[a] Structures were obtained from the CSD.[39] [b] Axial. [c] Equatorial. [d] The square residue errors reported here are for the single-point MXAN calculations.

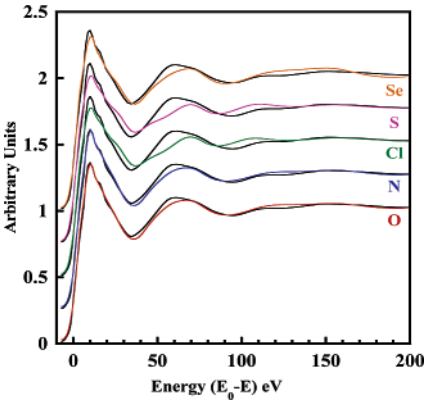

Figure 5. Cu K-edge XAS data of $[Cu^{II}(TMPA)(OH_2)](ClO_4)_2$ (black) and MXAN simulations involving change in the O_{ax} (axial H_2O) (red) to N_{ax} (purple), Cl_{ax} (green), S_{ax} (red), and Se_{ax} (orange) all at the same distance. The best simulation replacing O_{ax} is obtained for N_{ax} since the scattering amplitude of nitrogen is similar to that of oxygen.

Cu−L (N, Cl, S, and Se) bond distance of 1.97 Å, the errors were considerably worse than that for the best-fit simulation using the correct bond length of **1** (Table 2).

To test the sensitivity of MXAN to small structural changes, two sets of simulations were performed on a series of $[Cu^{II}(TMPA)L]^{n+}$ (L = ligand) complexes. In the first set, crystal structures of eight $[Cu^{II}(TMPA)L]^{n+}$ complexes were modified to replace L with O at 1.98 Å. The resulting structures have differences in the TMPA ligand moiety, brought about by varied interaction of Cu with L, which should result in differences in simulation results. The molecules were chosen to include both small and large perturbations in the first-shell ligation of the TMPA ligand with Cu relative to **1** (Table 2). Single-point MXAN calculations were performed using each modified crystal structure and the resulting spectra compared to the experimental spectrum of **1**. The simulations for four of the eight structures, $[Cu^{II}(TMPA)(F)](PF_6)$ (**2a**),[41] $[Cu^{II}(TMPA)$-OPO_2-(O-*p*-nitrophenyl)$Zn^{II}(TMPA)](BPh_4)$ (**2b**),[42] $[Cu^{II}(TMPA)$-$(NCMe)](ClO_4)$ (**2c**),[43] $[Cu^{II}(TMPA)$-O−$(F_8TPP)Fe^{III}](ClO_4)$ (**2d**),[44] and comparison to the experimental data are presented in Figure 6. The error, R_{sq} (eq 1), in these simulations is higher than in the single-point simulation using the actual crystal structure of **1** (Table 2). The largest error is obtained

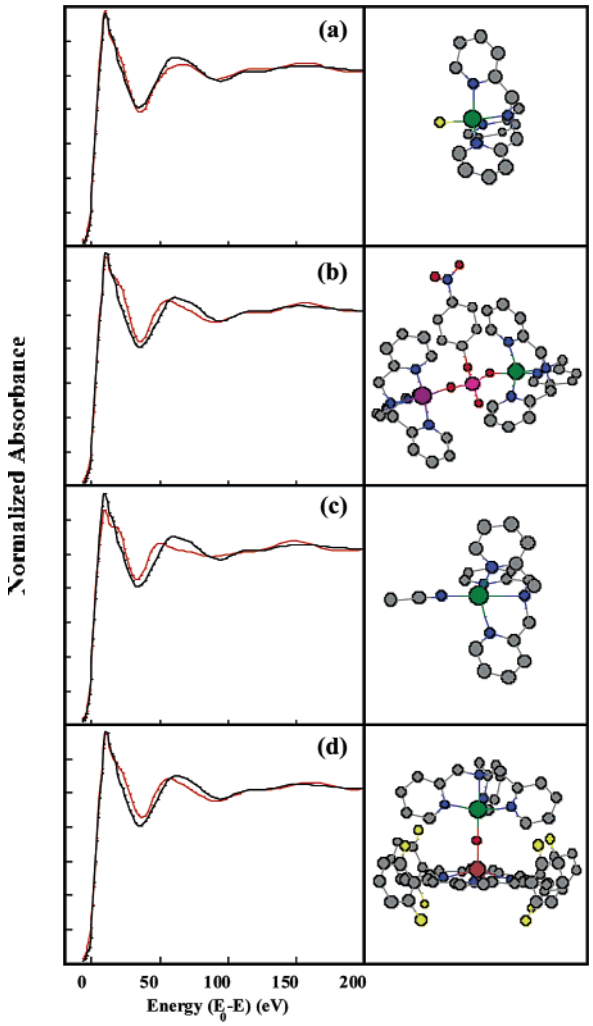

Figure 6. Cu K-edge XAS data of $[Cu^{II}(TMPA)(OH_2)](ClO_4)_2$ (black) and MXAN calculations (red). The structures used in the simulations corresponding to **2a**, **2b**, **2c**, and **2d** (see text) were modified from [Cu(TMPA)L] to [Cu(TMPA)(O)].

in the simulation using the modified crystal structure of **2c**, which contains a long equatorial Cu−N distance of 2.43 Å compared to 2.07 Å in **1.** These results clearly demonstrate the sensitivity of the MXAN method to changes in the first-shell bond distances. In the second set of simulations (Figure 7), the actual crystal structures of the eight complexes were used to correlate the ability of MXAN to distinguish between different models. This set of simulations, as expected, results in higher error than the previous set due to the greater deviation from the original crystal structure. The errors are reported in Table 2. The biggest change in the error value is observed for **2a** in going from the modified to the original

(41) Jacobson, R. R.; Tyeklár, Z.; Karlin, K. D.; Zubieta, J. *Inorg. Chem.* **1991**, *30*, 2035−2040.
(42) Adams, H.; Bailey, N. A.; Fenton, D. E.; He, Q.-Y. *J. Chem. Soc., Dalton Trans.* **1997**, 1533−1540.
(43) Lim, B. S.; Holm, R. H. *Inorg. Chem.* **1998**, *37*, 4898−4908.
(44) Karlin, K. D.; Nanthakumar, A.; Fox, S.; Murthy, N. N.; Ravi, N.; Huynh, B. H.; Orosz, R. D.; Day, E. P. *J. Am. Chem. Soc.* **1994**, *116*, 4753−4763.

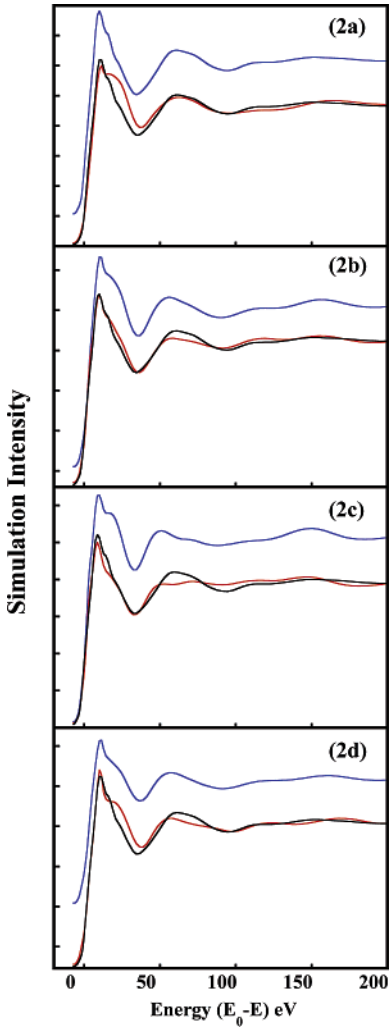

Figure 7. Cu K-edge XAS data of $[Cu^{II}(TMPA)(OH_2)](ClO_4)_2$ (black) and MXAN fit (red) to structures **2a**, **2b**, **2c**, and **2d**, respectively (Figure 1). The spectrum shown in blue is the corresponding modified structure simulation from Figure 1 shown here for comparison.

crystal structure. This is due to the short Cu−F interaction, 1.85 Å, which has a strong influence on the MXAN simulation. A short Cu−O bond also demonstrates considerable sensitivity as seen in the dramatic change in the R_{sq} values as Cu−O distance shortens (vide supra). These two sets of simulations demonstrate the ability of MXAN to distinguish small structural changes, while the first set of simulations demonstrates the ability of MXAN to distinguish changes in *Z* of one of the first-shell ligands in an otherwise constant ligand environment. This initial study thus shows very promising results on the application of MXAN to the study of low-symmetry biologically relevant molecules. Future studies will involve refinement of all structural and nonstructural parameters vs XANES data for a more extensive series of model complexes.

Conclusions

This study presents a systematic approach to determine the impact of structural changes on the XANES region of an X-ray absorption spectrum and applies the edge simulation package MXAN for the first time to a bioinorganic molecular model complex. The sensitivity of MXAN to small structural changes and specific atom replacements was tested. The results indicate that, with proper attention to goodness-of-fit measures and visual comparisons, MXAN can be used with confidence to extract structural information from the XANES spectrum. With further systematic development and testing, this multiple scattering approach can eventually be applied to biological systems of unknown metal-containing active-site structures to further elucidate structural correlation to function.

Acknowledgment. This work was supported by NIH Grant Nos. RR-01209 (K.O.H.) and DK31450 (E.I.S.). SSRL operations are funded by the Department of Energy, Office of Basic Energy Sciences. The SSRL Structural Molecular Biology program is supported by the National Institutes of Health, National Center for Research Resources, Biomedical Technology Program and by the Department of Energy, Office of Biological and Environmental Research**.** M.B. acknowledges financial support from SSRL for a two month stay as visiting scientist. The authors thank Prof. K. D. Karlin, Johns Hopkins University, for providing the model complex employed in this study.

Supporting Information Available: Figure displaying EXAFS data and best fits, and Fourier transforms of data and fit; Table providing numerical EXAFS fit results. This material is available free of charge via the Internet at http://pubs.acs.org.

IC050703N